Measurement of the time-resolved reflection matrix for enhancing light energy delivery into a scattering medium

Youngwoon Choi[1,2], Timothy R. Hillman[1],Wonjun Choi[2], Niyom Lue[1],

Ramachandra R. Dasari[1], Peter T. C. So[1,3], Wonshik Choi[2,*] and Zahid Yaqoob[1]

[1]*Laser Biomedical Research Center, G. R. Harrison Spectroscopy Laboratory, Massachusetts Institute of Technology, Cambridge, Massachusetts 02139, USA*

[2]*Department of Physics, Korea University, Seoul 136-701, Korea*

[3]*Mechanical and Biological Engineering Departments, Massachusetts Institute of Technology, Cambridge, Massachusetts 02139, USA*

Experimental scheme for detecting the spatial distribution of backscattered light

In order to determine the spatial distribution of time-resolved backscattered light from a turbid medium, we installed a line-field detection setup at the second detection port of BS3; the first port being used to acquire TRRM data (see Fig. S1(a)). Similar to the pinhole in Fig. 1, a slit S is placed in a plane that is conjugate to the sample plane for the line-field detection. The slit defines 1-dimensional detection line in the sample plane. The reference beam path is diverted using two folding mirrors (FM1 and FM2); a cylindrical lens CL is used for reference beam mode matching into the detection slit. The 1-D line shape of the combined sample and reference beams is converted into a 2-D distribution in the detection plane of the spectrometer that is composed of an imaging lens system and a grating G. The interference image is taken by a 2-D camera C3; a typical raw image is displayed in Fig. S1(b). This image is processed to retrieve a time-resolved line-field image, i.e., lateral scattered field distribution versus arrival time, as shown in Fig. S1(c).

Enhanced amplitude and TRRM reconstruction

By applying the complex amplitudes of all the phase ramps with their amplitudes assigned in Eq. (2) in the main text, we can obtain the amplitude of the reflected signal maximized at the arrival time $j_0\Delta t$:

$$\left|S_{opt}(j_0\Delta t)\right| = \sqrt{\sum_{i=1}^{N}\left|r(\vec{k}_i, j_0\Delta t)\right|^2}, \tag{S1}$$

where $\left|S_{opt}(j_0\Delta t)\right|$ is the detected amplitude after the optimization, $r(\vec{k}_i, j_0\Delta t)$ the measured TRRM element for i^{th} phase ramp and $j_0{}^{\text{th}}$ time bin, and N the total number of phase ramps used for the optimization. For the input wave given by Eq. (1) and Eq. (2) in the main text, which optimizes the intensity at arrival time of $t_0 = j_0\Delta t$, the complex field associated with backscattered wave at an arbitrary arrival time $t = j\Delta t$ also can be calculated as

$$\left|S_{opt}(j\Delta t)\right| = \sum_{i=1}^{N} r^*(\vec{k}_i, j_0\Delta t) r(\vec{k}_i, j\Delta t) \Big/ \sqrt{\sum_{i'=1}^{N}\left|r(\vec{k}_{i'}, j_0\Delta t)\right|^2}. \tag{S2}$$

The green and red curves in Fig. 3 in the main text were obtained using the above equation.

We also experimentally investigate the enhanced amplitude at the target arrival time as a function of N. Figures S2(a)-(c) show the peak signal growth in Figs. 3(a)-(c), shown in the main text, with increasing N. The two theoretical expectations (green and red curves) of TRRM reconstruction steadily increase; they achieve good agreement with a curve taking the form N^{α}, with α about 0.5[1]. This finding conforms to the theoretical predictions. In our experiment the backscattered signal is enhanced fairly well up to $N \sim 400$ and is in excellent agreement with the theoretical TRRM reconstruction, especially when using phase-only control. Beyond $N \sim 400$, however, the experimental curve exhibits saturation due to the inability of the SLM to generate finer patterns.

Detected signal (backscattered wave) vs. number of input channels

To quantify the role of the number of input channels on detected signal enhancement, we start by measuring S_{opt} for a specific time bin $j_0\Delta t$ as a function of N, the number of input channels (phase ramps) used for the optimization. The result is shown as a log-log plot in Fig. S3. The optimized signal increases monotonically with the number of input phase ramps up to $N \leqq 400$. However, as N

increases beyond 400, the tendency of signal growth deviates from the linear behavior; moreover, this discrepancy becomes larger with *N*. This is due to the lack of ability to display higher resolution phase maps on the SLM for larger values of *N*. In other words, as *N* increases the final optimized phase pattern becomes finer and more complicated. The pixelated structure of the SLM and its finite fill factor cause imperfection when writing such phase patterns on the SLM [2]. We, therefore, fit the data up to $N = 400$ with a line for predicting the role of number of input channels on reflected signal growth. As shown in Fig. S3, the data points are closely distributed near the fit line, yielding a slope of 0.47 ± 0.01 that is quite close to the theoretical expectation value of 0.5.

Reflection / transmission enhancement for various sample thickness

To characterize enhancement in backscattered and forward scattered light using TRRM, we prepared several samples with various thicknesses but with the same transport mean free path. Specifically, we chose sample thicknesses *L* of 86.5, 158.2, 232.6, and 376.6 μm that provided $2L/l_c'$ as 0.44, 0.84, 1.18 and 1.91, respectively. Here, l_c' is the transport mean free path. We note that these samples cover weak to moderate turbidity regime. The data presented in the main text (Figs. 2-4) was obtained using the thickest sample mentioned above. In this supplemental document, we present additional information about energy enhancement in reflection and transmission case using samples of smaller thickness.

Similar to our approach mentioned in the main text, we set the target time bin such that the arrival time corresponds to the back surface of each sample and then perform the optimization procedure for the reflected wave that corresponds to the target arrival time. The line-field distribution of the reflected wave was measured before and after the optimization (Figs. 4 (b) and (d) in the main text). Next, the ratio of energy associated with the light from target arrival time was calculated. Moreover, the energy change in the light transmitted through the back surface was also measured. Figure S4 summarizes our experimental observation of the relative energy enhancement in reflection and transmission cases for various sample thicknesses. For the thinnest sample used in the experiment

($2L/l_c'$ = 0.44), the energy enhancement for the reflected light (with the target arrival time) and that for the transmitted light were measured to be 100% and 41%, respectively. As the sample thickness increases, the enhancement values decrease monotonically. For $2L/l_c'$ = 1.91, the energy enhancement was measured as 41% and 20% for reflection and transmission cases, respectively. As mentioned in the main text, the correspondence between arrival time and the target depth is degraded with increasing $2L/l_c'$. Consequently, the ability to deliver energy to the target depth decreases with increasing sample thickness.

Random matrix theory for double-transmission configuration

In the main text, we observed that the optimization process increases both the energy of reflected light with a certain target arrival time and the total transmitted energy through the back surface of the turbid medium. Here we present a simple model for this rather counter-intuitive phenomenon using the random matrix theory (RMT). When a turbid medium is illuminated with incident light, in general, four waves are coupled to each other as shown in Fig. S5(a). This coupling can be described by the scattering matrix S as [3]:

$$\begin{pmatrix} E_a^- \\ E_b^+ \end{pmatrix} = S \begin{pmatrix} E_a^+ \\ E_b^- \end{pmatrix} \equiv \begin{pmatrix} r_{aa} & t_{ab} \\ t_{ba} & r_{bb} \end{pmatrix} \begin{pmatrix} E_a^+ \\ E_b^- \end{pmatrix}, \tag{S3}$$

where indices (a, b) denote each surface of the sample and the symbols (+, –) represent waves propagating from left to right and vice versa. Considering only one incident beam E_a^+ (E_b^-), t_{ba} (t_{ab}) will represent the transmission matrix for the direction left → right (right → left) and r_{aa} (r_{bb}) as the reflection matrix at the surface a (b). For a relatively weak turbid medium, the arrival time is related to the depth information of the sample to a large extent. So if we perform a time-resolved detection for reflected light, and we narrow down our focus only on a specific arrival time from within the turbid medium, then the majority of detected signal will be related to the reflected wave originating from the depth associated with the target arrival time. Figure S5 schematically represents this idea. As shown in Fig. S5(a), if we set the target arrival time $t_0 = 2nL/c$, where L is the sample thickness, c is

the speed of light in vacuum and n is the mean refractive index of the medium, then the light reflected from the back surface of the sample is taken into account preferentially. This reflected light undergoes the same medium twice such that the total propagation distance is $2L$. We can consider this *two-way single reflection* geometry as *one-way double transmission* configuration (see Fig. S5(b)). In this model, the total thickness of the turbid medium remains $2L$, and the microscopic distribution of scattering particles inside the medium shows mirror symmetry with respect to the central line of the medium.

Now we can describe the reflection of light from the medium using the transmission matrix. In Fig. S5(a), if we set the transmission matrix of the medium from the left to the right side as t_{ba}, then the transmission matrix for the reverse direction will be given as t_{ab}. Correspondingly, the sequence of two transmissions in Fig. S5(b) will be described simply by these two matrices as:

$$T = t_{ab} t_{ba}. \tag{S4}$$

The reflected light *at the target depth* can now be described by the modified transmission matrix.

Next, we numerically generate a full scattering matrix S for a disordered medium with certain turbidity. The matrix S is constructed with 2000 by 2000 elements such that its eigenvalue distribution satisfies the random matrix theory (RMT). From the submatrices of S, we calculate the double transmission matrix T given by Eq. (S4) and perform the single-channel optimization using T. This simulates our experimental situation where the light with a certain target arrival time is optimized in a moderately turbid medium. Therefore, the energy enhancement at port a after the optimization is calculated as:

$$\eta_{ref} = \frac{\left|TE_{opt}\right|^2}{\left|TE_0\right|^2} - 1, \tag{S5}$$

where E_{opt} and E_0 are incident light field with and without single-channel optimization. Note that this reflection enhancement corresponds only to the light with specific arrival time. We also calculate the enhancement in the transmitted energy (at port b) using the same input wave E_{opt} as:

$$\eta_{tr} = \frac{\left|t_{ba}E_{opt}\right|^2}{\left|t_{ba}E_0\right|^2} - 1. \tag{S6}$$

In Figure S6, we have calculated the ratio of enhancement defined by

$$\frac{\eta_{tr}}{\eta_{ref}}, \tag{S7}$$

for a range of turbidity values including the ones used in our experiment. The data points are closely distributed to the value of 0.5 over the whole range of our calculation. This result indicates that the transmitted energy (or the energy delivered to a target depth) is enhanced by approximately half of that in reflection. Since the optimization is performed using the total matrix T for the reflection, the energy enhancement for the transmission is less effective. Our experimental data, depicted in the Fig. S6, is also in good agreement with the numerical curve.

Although we made a time-gated detection, we find that the RMT theory describing the steady-state interaction of light with a turbid medium can still be applied to interpret our experimental results. If the target arrival time t_0 is set not too far beyond the reduced scattering time $t_{\mathrm{rst}} = nl_c'/c$, the one-way double-transmission configuration holds valid. However, when $t_0 \gg t_{\mathrm{rst}}$, the correspondence between arrival time and depth information is lost, thereby rendering the double-pass transmission model inappropriate.

Preparation of a turbid medium (type I & type II sample)

For the experiments reported in the main text, the turbid medium (type I sample) was prepared using polydimethylsiloxane (PDMS, Dow Corning, Sylgard 184) and polystyrene beads of 4.5 μm diameter (Duke Scientific, Polymer Microspheres-7505A). The beads were mixed into the PDMS to obtain final concentration of 4.8×10^{-4} μm^{-3}. The scattering mean free path of the turbid sample was measured to be l_c = 35.9 ± 0.2 μm and the transport mean free path l_c' = 394.3 ± 2.0 μm, through ballistic wave propagation detection [4] which was in good agreement with the value predicted by Mie scattering theory. With the same medium, we prepared four samples with different thicknesses. The measured sample thicknesses L were 86.5 μm, 158.2 μm, 232.6 μm, and 376.6 μm,

corresponding to the numbers of reduced scattering events, $2L/l_c'$, 0.44, 0.84, 1.18, and 1.91, respectively.

For the complementary experiments shown in Fig. S7, we prepared another scattering medium (type II sample) by mixing polystyrene beads with three different sizes of 1, 3, and 5 μm in PDMS so that the medium was more complicated and more turbid than the type I sample for the experiments reported in the main text. The scattering mean free path and the transport mean free path of the type II turbid sample were measured to be l_c = 19.4 ± 0.9 μm and l_c' = 138.4 ± 1.1 μm, respectively. We cured the medium in the form of layers with different thicknesses, 233.8 μm, 306.4 μm, and 397.3 μm corresponding to $2L/l_c'$ = 3.38, 4.43, and 5.74, respectively.

Preparation of biological specimens (type III sample)

In order to demonstrate the ability of our technique for enhancing light energy delivery through biological specimens, we used chicken breast tissues as scattering media. For this purpose, we fixed a bulk of chicken breast tissue following the standard fixation protocol. We first sliced a chicken breast tissue into small pieces with a thickness less than 3 mm and washed them using phosphate buffered saline (PBS) solution. Next, the tissue samples were immersed in 10 % diluted formalin solution and stored overnight at 4 ^{o}C. After fixing the bulk tissue, we cut them into thinner slices and press them between a slide glass and a cover slip. The scattering mean free path and the transport mean free path of the fixed chicken breast tissue were measured to be l_c = 67.6 ± 2.9 μm and l_c' = 395.8 ± 3.6 μm, respectively. We prepared two tissue slices with thicknesses of 339.7 μm and 586.4 μm corresponding to $2L/l_c'$ = 1.72 and 2.97, respectively.

Transmission enhancement with different types of samples

We performed the reported optimization procedure on type II and III samples and observed the energy enhancement in both cases. The observed transmission enhancements for various samples with N = 1600 are shown in Fig. S7. Blue circles correspond to the results obtained with type I sample (the

main results shown in Fig. S4), red squares illustrate transmission enhancement with type II sample, and black triangles show energy enhancement obtained with the chicken breast tissues (type III sample). With type II samples, we observed 10.2 % and 2.5 % enhancements for $2L/l_c'$ = 3.38 and 4.43, respectively. However, for the sample with $2L/l_c'$ = 5.74, no noticeable enhancement was observed. We believe that this is the limitation of our current technique for delivering enhanced light energy through a scattering medium. With the type III samples, the fixed chicken breast tissue slices, we obtained 27.4 % and 5.7 % enhancements for $2L/l_c'$ = 1.72 and 2.97, respectively.

Control of spatial light modulator (SLM) for construction of TRRM

Each incident channel for independent input wave is generated by writing an appropriate linear phase ramp containing an integer number of cycles in the vertical and horizontal directions. The phase ramp is applied to a square active area (350X350 pixels) of the SLM (Hamamatsu, LCOS-SLM X10468-02). This sub region of the SLM fills the entire back aperture of the objective lens (OL1 in Fig. S1). We measured the time-gated backscattered signals from the sample for all the generated phase ramps in a sequential manner and constructed sample's TRRM by gathering all detected signals. The measured complex fields have different speckle realizations due to sample turbidity. Only a single measurement is required for each channel of illumination because of the complex field recording via interferometric detection. This efficiently increases the measurement speed compared to phase-stepping approach [5]. The maximum number of phase ramps used in our experiment is 1600; the total scanning time is about 160 seconds, a quantity that is determined primarily by the access time of the SLM (~50 msec).

References

1. I. M. Vellekoop and A. P. Mosk, "Focusing coherent light through opaque strongly scattering media," Opt Lett **32**, 2309-2311 (2007).
2. M. Kim, Y. Choi, C. Yoon, W. Choi, J. Kim, Q.-H. Park, and W. Choi, "Maximal energy transport through disordered media with the implementation of transmission eigenchannels," Nat Photonics **6**, 581 (2012).

3. R. Mittra and T. M. Habashy, "Theory of Wave-Front-Distortion Correction by Phase Conjugation," J Opt Soc Am A **1**, 1103-1109 (1984).
4. Z. Yaqoob, D. Psaltis, M. S. Feld, and C. Yang, "Optical phase conjugation for turbidity suppression in biological samples," Nat Photonics **2**, 110-115 (2008).
5. S. M. Popoff, G. Lerosey, R. Carminati, M. Fink, A. C. Boccara, and S. Gigan, "Measuring the Transmission Matrix in Optics: An Approach to the Study and Control of Light Propagation in Disordered Media," Phys Rev Lett **104**(2010).

Supplemental Figures

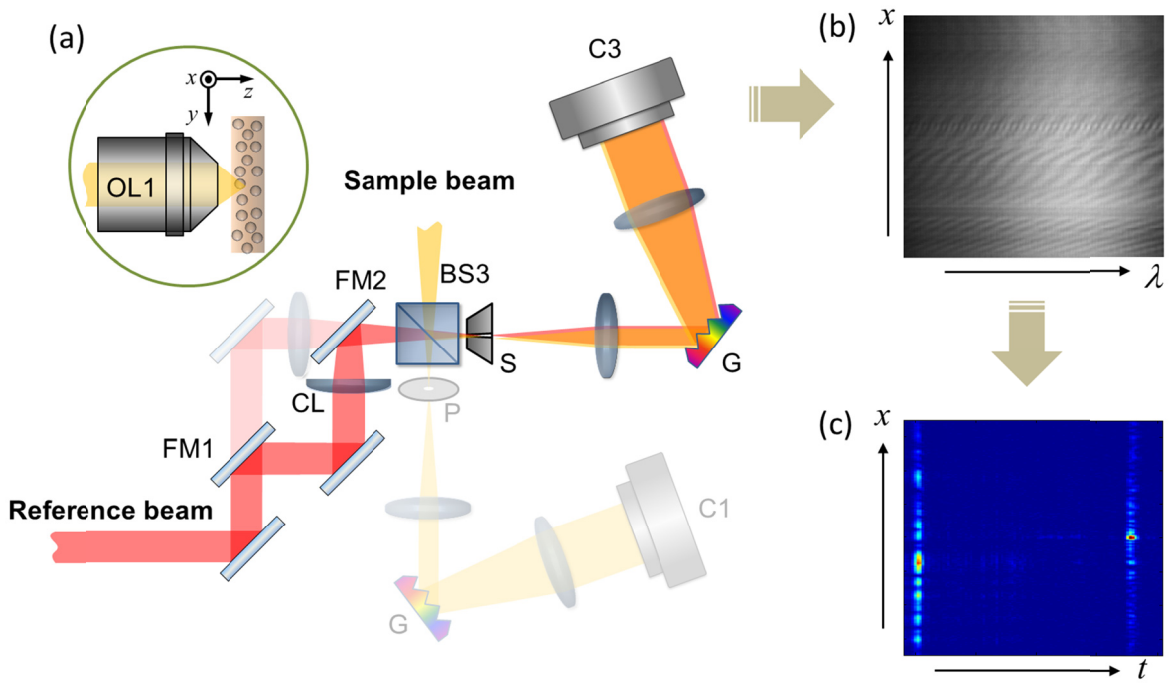

Figure S1. Detecting spatial distribution of backscattered light from a turbid medium. (a) Schematic diagram for the line-field detection setup to measure the backscattered wave from the sample along a line. The sample beam reflected by BS3 is used for this purpose. Slit S, defining the sampling line, is positioned at the conjugate plane of the sample plane. Two fold mirrors FM1 and FM2 make a detour for the reference beam when the line-field distribution is measured. Furthermore, the reference beam is shaped by a cylindrical lens CL for matching mode into the slit S. Inset represents the spatial coordinate on the sample plane. The subdued components form the detection setup for TRRM measurement, as described in the main text. (b) A typical interference image taken by the camera C3. Vertical and horizontal axes represent long side of the slit and wavelength axis, respectively. (c) A line-field image after converting wavelength dimension into the arrival time; the vertical and horizontal axes represent lateral and time dimensions, respectively.

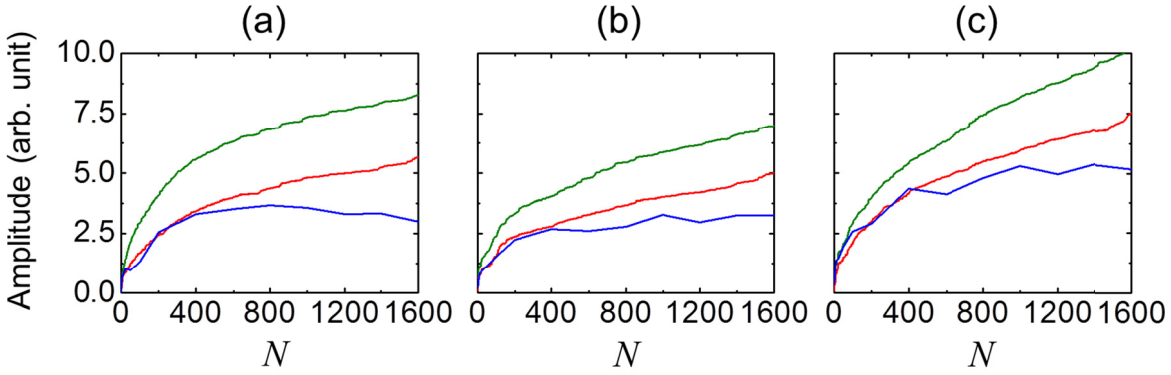

Figure S2. Reflection signal enhancement and TRRM reconstruction. (a)-(c) Signal enhancement at the same arrival times as Fig. 3(a), (b), and (c) in the main text, respectively, as a function of the number of input channels N. Blue lines: measured time-gated signal with phase-only control of incident wave. Green lines: theoretically expected reflection signal estimated by Eq. (S1). Red lines: the same as green lines but with the phase-only input.

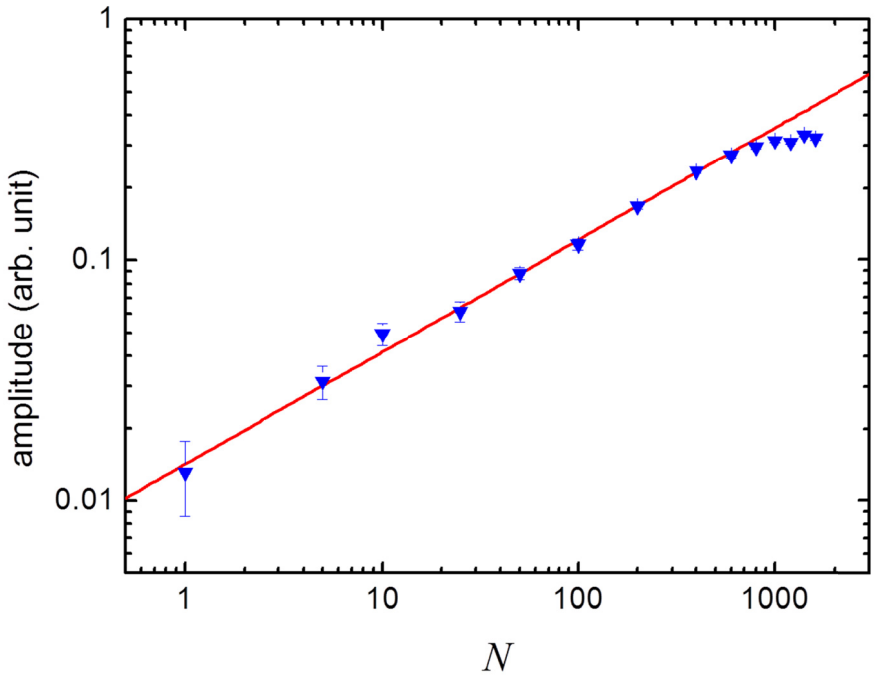

Figure S3. Reflected signal growth as a function of input channels. The amplitude of reflected wave at a fixed time bin $t_0 = j_0\Delta t$ is measured as a function of N, the number of phase ramps, after optimizing the same time bin t_0. Blue dots are the experimental data whereas the red line represents a linear fit. The slope of the fitting line is 0.47 ± 0.01 showing a good agreement with the theoretical prediction. Only the data points $N \leq 400$ are used for the fit.

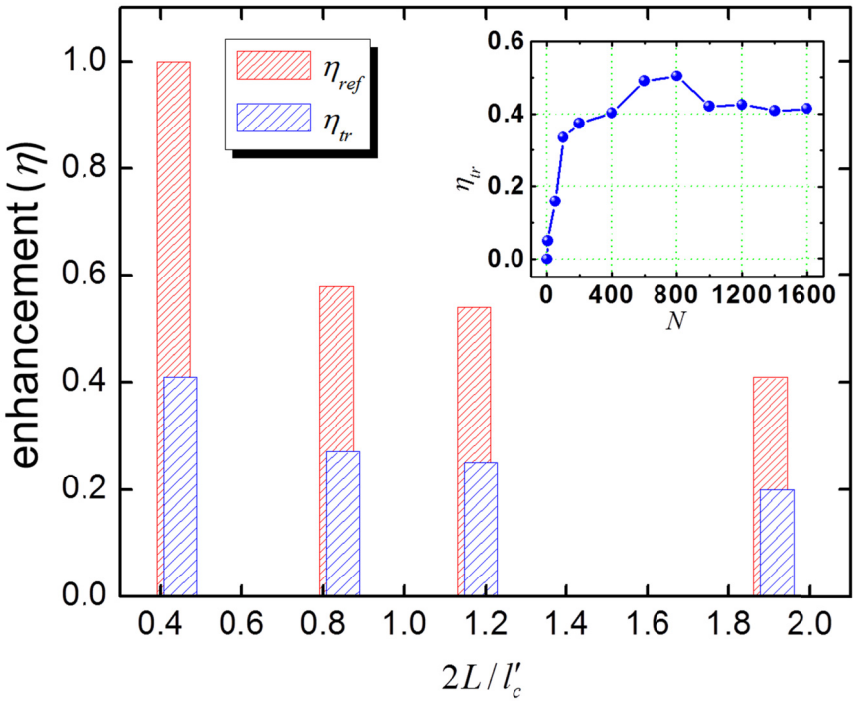

Figure S4. Reflection enhancement (η_{ref}) and transmission enhancement (η_{tr}) via single-channel optimization process for various sample thicknesses. As explained in the main text, the target arrival time for the reflection signal is set in a way that the corresponding depth coincides with the back surface of each sample. The relative enhancement factors are measured for both the reflection and transmission cases. For the reflection enhancement, only the energy contained in the target time bin is considered. However, total energy is taken into account for the transmission case. Both enhancement factors decrease with increasing sample thickness. The inset represents the transmission energy enhancement for the thinnest sample as a function of N. The final enhancement is 41% for N=1600.

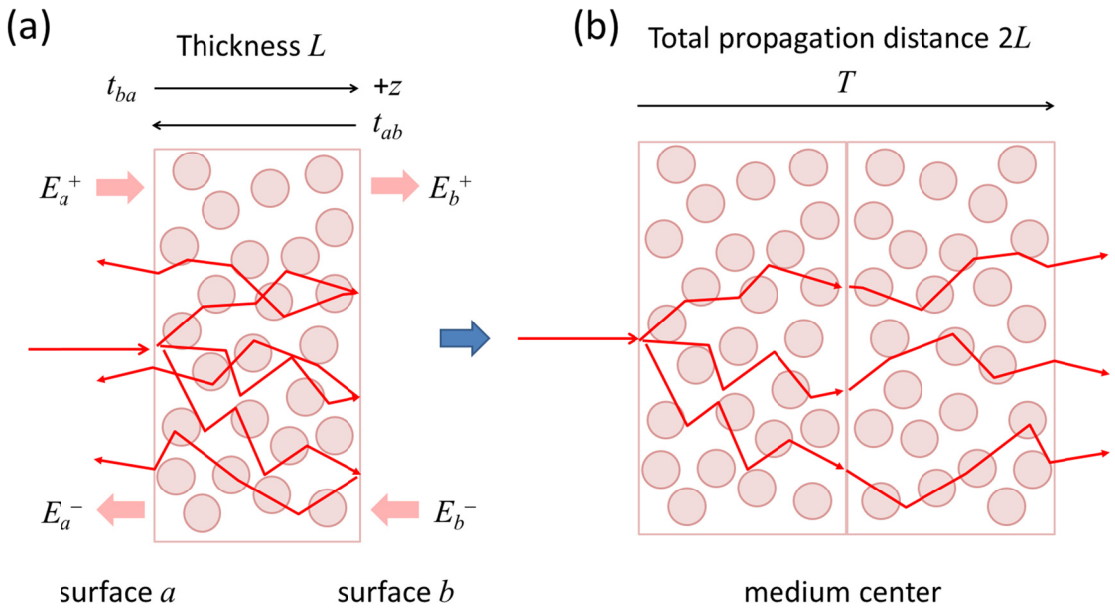

Figure S5. Double-transmission configuration to model reflection signal enhancement. (a) A scenario showing reflected signal arising from the back surface of the turbid medium, which can be interpreted as light wave propagation through the same medium twice – at first in the forward ($+z$) direction and then in the backward ($-z$) direction. Each transmission is described by the transmission matrices t_{ba} and t_{ab} of the medium, respectively. (b) Representation of reflection geometry as a double-transmission configuration. The light propagates through a series of two media with mirror symmetry with respect to the central line. The light propagation is described by the total double transmission matrix T of the medium, which is described by t_{ba} and t_{ab}, with the thickness of $2L$. This model is valid if the target depth is of the same order as the reduced scattering length of the sample.

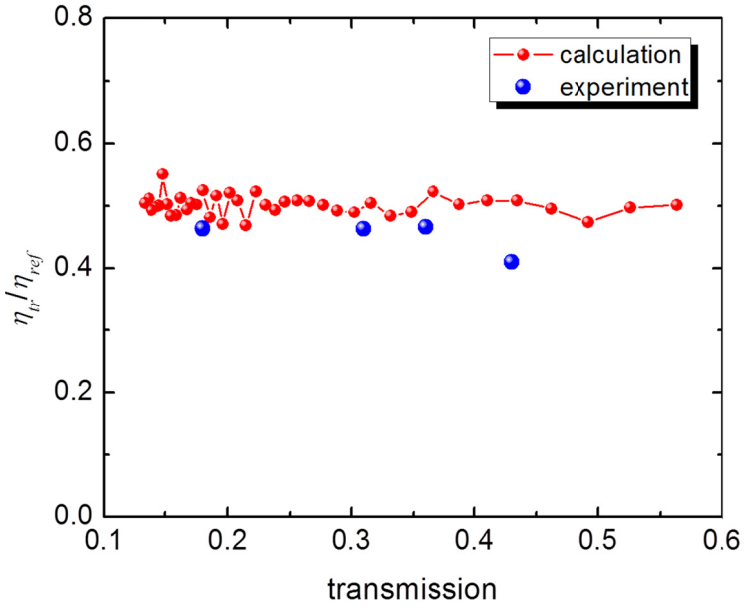

Figure S6. Comparison between transmission and reflection enhancements. The energy enhancement for reflection (η_{ref}) and transmission (η_{tr}) cases is calculated using Eq. (S5) and Eq. (S6), respectively. Next, the ratio of enhancement, defined by Eq. (S7) is obtained as a function of sample turbidity represented as the mean transmittance of samples without any wavefront control. The ratio of net enhancement stays near the value of 0.5 over the whole range of our calculation. Blue dots represent our experimental data, which is quite close to the predicted values derived from the double-transmission model.

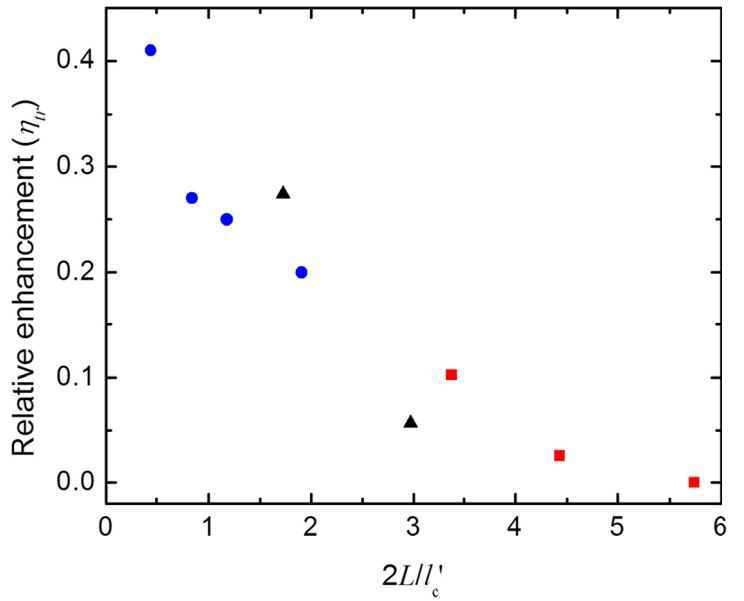

Figure S7. Transmission enhancements (η_{tr}) using different types of samples (see the above text for sample preparation). Blue dots represent the transmission enhancement obtained with type I samples, also depicted in Fig. S4. Red squares correspond to the transmission enhancement obtained with type II samples. Black triangles represent transmitted energy enhancement with type III samples, i.e., fixed chicken breast tissue samples.